June 2025

$\Xi - \bar{\Xi}$ triggered $K/(\pi^+ + \pi^-)$ Yield Ratio: unveiling the microscopic hadronization mechanism

Rayan Rabbani

Theoretical Particle Physics
Division of Particle and Nuclear Physics
Department of Physics
Lund University

Bachelor thesis (15 hp) supervised by Christian Bierlich

LUND
UNIVERSITY

Abstract

This thesis investigates the $K^{\pm}/(\pi^{+}+\pi^{-})$ yield ratio near $\Xi-\bar{\Xi}$ pairs in pp collisions at mid-rapidity ($|\eta|<1$) to distinguish between two competing models of strangeness enhancement: the rope hadronization model, implemented in PYTHIA, and the canonical statistical hadronization model, implemented in Thermal-FIST. The results from both models show strong agreement with experimental data from the ALICE Collaboration for strangeness enhancement in strange hadron-to-pion yields. By analyzing $(K^{+}+K^{-})$ and $(K^{\pm})$ yields normalized to $(\pi^{+}+\pi^{-})$ near Ξ and $\bar{\Xi}$ separately, the study tries to distinguish the microscopic and macroscopic mechanisms of hadronization. A clear distinction is observed in the K/π ratios near $\Xi-\bar{\Xi}$ pairs at low multiplicities. PYTHIA predicts higher K/π yields than Thermal-FIST. At high multiplicities, PYTHIA shows a lower K^{+}/π and K^{-}/π yields than Thermal-FIST, where Thermal-FIST shows a gradual rise in strangeness enhancement. The findings suggest that further refinement in rapidity ranges and larger datasets are needed to clarify the distinctions between the models. This work contributes to understanding the underlying frameworks of strangeness production in high-energy collisions.

Popular Science Summary

Physicists have spent much of the past 5 decades smashing particles together, at nearly the speed of light, to understand the fundamental rules that define the universe in which we live. These high-energy collisions, conducted in particle accelerators such as the Large Hadron Collider (LHC) at CERN, create a cascade of new particles. A part of these new particles contain "strange" quarks, which are an exotic type of matter that are not typically found in ordinary atoms that make up the known universe. 'Strangely' enough, in 2016, the ALICE Collaboration found that colliding high-energy protons, which together with neutrons form the atomic nucleus, produce more strange quarks than expected. This opened up a new mystery in physics known as **strangeness enhancement**.

Two theories lead to explain this mystery. One, called the **Quark-Gluon-Plasma** (QGP) *statistical hadronization model*, suggests that collision events briefly transform the event into a high-density 'soup-like' state where quarks and gluons mirror what existed moments just after the Big Bang. The other, known as the *rope hadronization model* or aptly called the **Lund model**, argues that the collision events producing new particles arise from colour fields or strings stretching and breaking, forming new particles. Multiple strings overlapping are together called a 'rope'.

Due to the difficulty in theoretically describing the experiments, phenomenology is used to reconstruct final-state particles from collision events. My thesis investigates the distinction the Lund and QGP models using PYTHIA (for the Lund model) and Thermal-FIST (for the QGP model) event generators. By comparing the results of these simulations with real experimental data from the ALICE Collaboration, we can understand which model better explains the strangeness enhancement.

In my thesis, we propose that the key distinction between the statistical model and the rope hadronization model is macroscopic versus the microscopic interactions of infinitesimally small particles. As the statistical model expects a quark-gluon-plasma to form, the model predicts strangeness enhancement via providing the probability distributions of all allowed final particles after the collisions; therefore, the model looks into the collision event macroscopically. The rope hadronization model, on the other hand, looks into the collision event as microscopic string breaks and forms new particles while still upholding current fundamental rules of physics. We believe that looking deeper into a chosen particle-antiparticle interaction in the collision event and analyzing the strange quarks that come from it would pose a valid argument for distinguishing the two models. This distinction in strangeness enhancement, along with further streamlined experiments from the ALICE Collaboration, may help posit a better understanding of the mysteries that currently lie in particle physics and may bring us one step closer to unlocking the fundamental nature of our known universe.

The appearance of strange quarks in high-energy collisions is a puzzle that challenges our understanding of the fundamental laws of physics. By testing competing theories with advanced simulations, we aim to determine whether strangeness enhancement in high-energy proton-proton collisions is caused by the Quark-Gluon-Plasma or by breaking tiny color strings. As my research continues, we move closer to solving this mystery.

Contents

List of acronyms

QGP - Quark-Gluon-Plasma
BSQ - Baryon-Strange-Charge

List of Figures

List of Tables

1 Introduction

During high-energy heavy-ion collisions, quarks and gluons are expected to exist in a dense deconfined state known as the quark-gluon plasma (QGP). Experimental observations conducted by the ALICE Collaboration have shown evidence for a deconfined QGP state in high-energy Pb-Pb collisions[1]. A key signature for this is the enhanced production of strange hadrons relative to pions, scaled with the increased event multiplicity classes. Multiplicity classes categorize collision events by the number of final-state particles detected. This phenomenon is known as *strangeness enhancement*. This acts as a probe for QGP properties and the underlying dynamics of partons under extreme conditions.

However, in proton-proton (pp) collisions, experimental observations conducted by the ALICE Collaboration in 2016[2] have demonstrated that the relative production of strange and multi-strange hadrons increases significantly as the event multiplicity increases. The observation suggested that QGP is also created in pp collisions. This was surprising since pp collisions do not meet the conditions required to form a QGP-like state. Two different theoretical models can explain this strangeness enhancement: rope hadronization (without QGP) and statistical hadronization (with QGP). Since they agree with the ALICE experiments' data, this thesis aims to distinguish between the two models.

The rope hadronization model[3] explains strangeness enhancement via microscopic interactions of strings to create hadrons after the collision. These strings are colour fields that connect quarks. The subsequent overlap of these strings is called a rope. The hadronization process occurs when the strings contain enough energy to break, forming new quark-antiquark ($q\bar{q}$) pairs. In high-energy collision events, these string breaks and the formation of new quarks and antiquarks can explain the increased production of strange-multistrange hadrons observed by the ALICE experiments. The model is incorporated into the Monte Carlo event generator PYTHIA[4], which will be used in this thesis.

The statistical hadronization model assumes macroscopic QGP-like conditions, as canonical ensembles, to predict hadron formation after the pp collision. Dense regions of quarks and gluons are allowed to interact with each other until these regions expand and cool until thermal and chemical equilibrium is reached. When the quarks and gluons stop interacting, it is called the '*freeze-out*' temperature. Hadron production is determined by the temperature and size of the volume reached at the freeze-out and the baryon, strangeness, and charge (BSQ) conservation laws. Additionally, strangeness production is suppressed by the strangeness saturation factor. The freeze-out temperature, volume, and strangeness saturation factor increase with increasing multiplicities. Ultimately, this increases the production yields of strange-multistrange hadrons. Thermal-FIST[5] implements the statistical hadronization model and will be used in this thesis.

This paper will analyze the production of kaons near $\Xi - \bar{\Xi}$ pairs to distinguish between the two models. In PYTHIA, the hadrons close to $\Xi - \bar{\Xi}$ pairs should be kaons with high probability due to local conservation of strangeness. Additionally, it is expected that the number of kaons increase with multiplicity due to the higher number of string breaks in the $\Xi - \bar{\Xi}$ productions. However, Thermal-FIST should conserve the strangeness globally, with Ξ and $\bar{\Xi}$ present in the $|\eta| < 1$ region. The kaons would then be normalized to the pions in the same area to give K/π ratios in both PYTHIA and Thermal-FIST.

2 Theory

Monte Carlo event generators use rope and statistical hadronization models to simulate pp collisions. PYTHIA and Thermal-FIST are the primary event generators used in this thesis. The former uses the rope hadronization model, whilst the latter uses statistical hadronization. This thesis aims to distinguish the models based on results taken from the two models.
PYTHIA uses the Lund model, explained in Section 2.2, to simulate the hadronization process in pp collisions. It is based on the formation of strings that decay into final-state hadrons, thus looking at the event from microscopic interactions between strings. The strings connect partons until they reach or decay into the final-state hadrons.
On the other hand, Thermal-FIST uses the statistical hadronization model, explained in Section 2.3.1, to simulate pp-collisions. Unlike PYTHIA, Thermal-FIST is a macroscopic thermodynamic event generator that assumes a thermalized medium or QGP from which particles are produced. Based on the statistical model, hadron yields are determined by the canonical ensemble where the system's temperature T, baryon chemical potential μ_B, strangeness saturation γ_s, and volume V are primary parameters considered. The final-state hadrons are derived from the primordial hadron probability distribution (initial thermally produced hadrons) and the probabilistic resonance (short-lived, unstable particles) decay chain. The theoretical basis for Thermal-FIST is presented as follows: the canonical statistical model (Section 2.3.2), and the Thermal-FIST parameters (Section 2.3.3).

2.1 PYTHIA

The microscopic model in PYTHIA goes through step-by-step procedures for the hadronization process from quarks and gluons to the final-state hadrons.

2.2 Lund Model: String Fragmentation

The Lund model describes hadronization through the formation and fragmentation of color fields, modeled by flux tubes or massless relativistic 'strings' stretched between a quark-antiquark ($q\bar{q}$) pair. A single string has a tension of approximately $\kappa \approx 1$ GeV/fm. As the string is stretched between separated colour charges, the $q\bar{q}$ pair reaches a break-point and fragments into one or two new pairs of quarks at the fragmentation points. Figure 1 shows the fragmentation of a singular string.

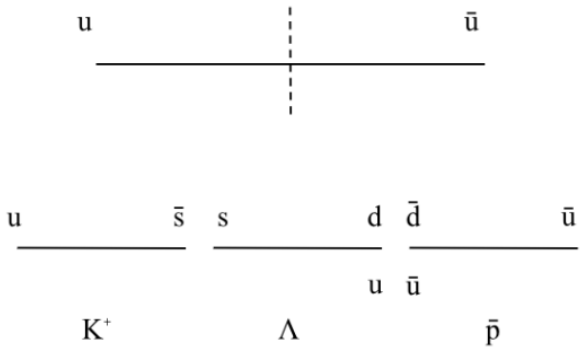

Figure 1: Sketch of a $u\bar{u}$ string break forming K^+, Λ, $\bar{p}$
hadrons with s from Λ balanced with the $\bar{s}$ from K^+ and the baryon number from Λ balanced by $\bar{p}$.

The string break that created the new pair in Figure 1 is a quantum tunneling process. The newly created $q\bar{q}$ pair tunnels through a potential barrier given by the pair's energy. It is important to note that the energy released in the string break is the energy that enters the tunneling process[6]. This energy is the mass and momentum of the $q\bar{q}$ pair. The probability of this transmission is given by equation (1):

$$T \propto \kappa \exp\left(-\frac{\pi m^2}{\kappa}\right) \tag{1}$$

Where m is the mass of the quark or diquark and κ is the string tension.
The transmission probability gives the probability of producing a quark of a certain mass. It can then be used to find the hadron yields.

2.2.1 Baryon Production

Expanding on the sketch in Figure 1, this section will explain the baryon production process. Colour charges of hadrons can take on the colour charge values, r (red), b (blue), g (green), and their corresponding anticolour charges. In the simplest case, a $q\bar{q}$ pair would have a subsequent colour field, called the string. All hadrons form a neutral colour charge such that colour-anticolour charge pairs, or r, b, and g colour charges together form the colour neutral charge *white*. The anticolour charges $(\bar{r}, \bar{b}, \bar{g})$ also form a colour-neutral state. This is called *colour confinement*.
Figure 2 describes the baryon production process using the popcorn model[7]. As a $q\bar{q}$ pair has a colour field between the two colour charges, random vacuum fluctuations between the pair can create other $q\bar{q}$ pairs of different colour charges. If a $g\bar{g}$ pair is formed between the $r\bar{r}$ pair, the red and green colour charges can appear like an antiblue antiquark, called a colour antitriplet. The field line is directionally opposite, moving from the colour triplet to the colour antitriplet. Then, if a secondary blue-antiblue $q\bar{q}$ pair forms within this field due to fluctuations, the blue quark will be dragged towards the colour antitriplet (antiblue and the antiblue quark will be dragged towards the colour triplet (blue). A string break in the fluctuation region, as in Step 3 in the popcorn model in Figure 2, can result in the production of a baryon-antibaryon $(B\bar{B})$ pair.

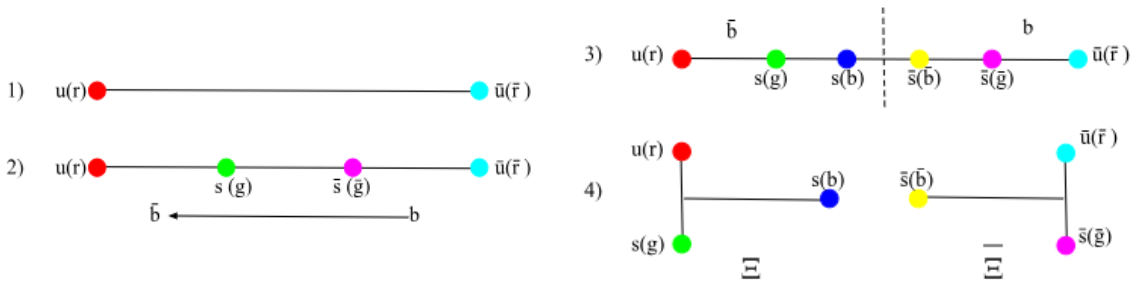

Figure 2: Step-by-step illustration of the popcorn model producing $\Xi - \bar{\Xi}$ pair.

The size and density of the fluctuations determine the rate of the $B\bar{B}$ pair production. However, experimental data have shown that additional mesons are produced between $B\bar{B}$ pairs, suggesting that large fluctuations form mesons between the pair that follow the same process described in this section. For example, in the case of Figure 2, a antiblue-blue $(\bar{b}b)$ ϕ meson in-between $(\bar{s}s)$ can be produced upon string breaks. These meson in-betweens have since been incorporated into the popcorn model.

2.2.2 Junctions

In contrast to the popcorn model, where $B\bar{B}$ are formed from single strings, junctions form $B\bar{B}$ pairs from multiple string interactions. After the initial collision, the parton shower goes through colour reconnection. Colour reconnection is how quarks and gluons in the parton shower form strings[4]. These strings are formed by minimizing their total energy, or length, following QCD rules. The strings can swap endpoints if it reduces their combined length, and sometimes three strings merge at a junction, forming a Y-shape. The resulting baryon, therefore, has three strings or "legs". This happens probabilistically based on colour matching, forming a colour-neutral state.

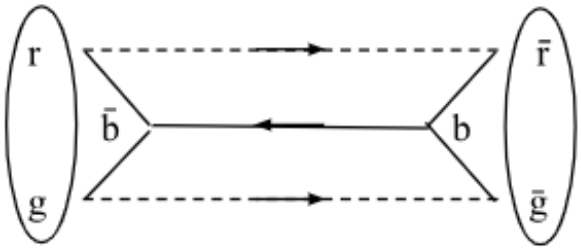

Figure 3: Illustration of the junction-antijunction formation process

Extending this concept to a junction-antijunction pair, such as in Figure 3, the red and green colour charges form the colour antitriplet ($\bar{b}$) at the junction point. The dashed lines are the respective single strings between $r\bar{r}$ and $g\bar{g}$ colour charges which are then translated to the directionally opposite colour field between the colour triplet-antitriplet pair at the junctions. Figure 4 shows the formation of a $\Xi - \bar{\Xi}$ pair from junctions. The legs not connecting the junction-antijunction pair are first fragmented iteratively. This forms a colour antitriplet (antiblue) diquark and a colour triplet (blue) antidiquark at the junction points. The remaining string connecting the diquark and the antidiquark can then be fragmented iteratively, ultimately producing a $B\bar{B}$ pair.

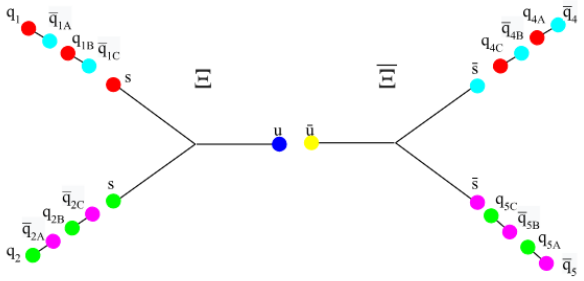

Figure 4: Illustration of junction dynamics for a $\Xi - \bar{\Xi}$ pair. Colour (shown in red, green, blue) and respective anticolour (shown in cyan, magenta, yellow) charges depict colour confinement.

2.2.3 Rope Hadronization: Multiple String Interactions

In a high-energy collision event, these strings can overlap. The overlapping strings produce a net colour field, called a rope. Figure 5 shows the different configurations of colour charges of $q\bar{q}$ pairs and their respective field lines. Case 1 shows arbitrary colour charges and their respective colour fields. Case 2 shows when the colour charges for the $q\bar{q}$ pair are the same.

The thick arrow is the increase in the net colour field strength. The energy density (or rope tension) increases by:

$$\kappa_{eff} = \frac{1}{4}\left(p^2 + 3p\right)\kappa \tag{2}$$

where p is the number of overlapping strings[3]. Case 3 is a trivial example, as explained in Section 2.2.2, where the overlapping strings create a colour antitriplet ($\bar{g}$) from the r and b colour charges and a colour triplet (g) for the overlapping anti-quarks. Hence, the colour field only flows in the opposite direction.

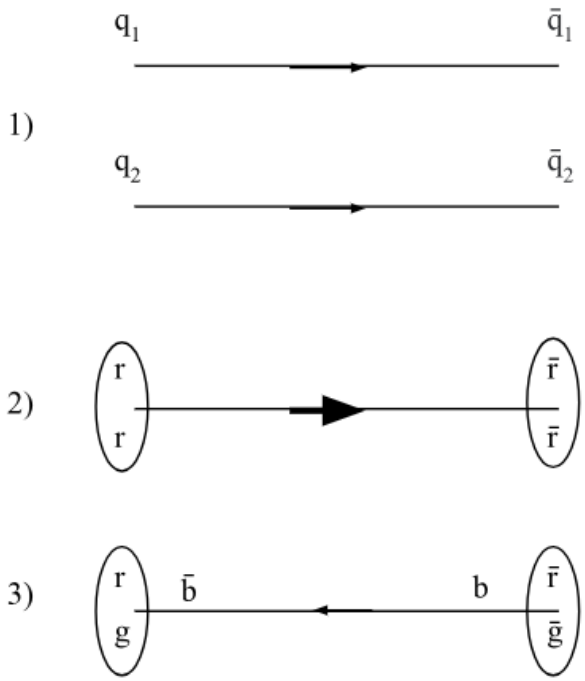

Figure 5: Multiple string interaction with arrows showing direction of the colour field. Case 1: Isolated $q\bar{q}$ strings with arbitrary colour charges. Case 2: Same colour charges within a string overlap. Case 3: Different colour charges within a string overlap (junctions, see Figure 3).

In reality, the transmission probability, equation (1), cannot be used to find the production yields of a specific quark. This is because quark masses are not properly defined. Instead, the parameter is set by comparing to experimental data from e^+e^- collisions. The transmission probability is used to derive the ratio between a heavier (s) quark and a light (u or d) quark, calling it the *suppression factor*[6]. The strangeness suppression factor becomes:

$$\rho = \frac{P_s}{P_{u,d}} = \exp\left(-\frac{\pi(m_s^2 - m_u^2)}{\kappa}\right) \tag{3}$$

Experimentally, the free parameter $\rho \approx 0.217$[4] from fits to data. This avoids using specific values for m_s, the strange quark mass, and m_u, the mass of the up quark.

When two overlapping strings form a rope ($p = 2$), the rope tension increases to $\frac{5}{2}\kappa$ from equation (2). When the rope breaks, the first string breaks with a string tension of $\frac{3}{2}\kappa$ and the remaining string would have a string tension of 1κ. This increased effective κ_{eff} replaces κ in equation 3. As κ increases, the probability of producing strange quarks increases. Therefore, in high multiplicity events, it can be observed that there is a strangeness enhancement. The full settings for PYTHIA used in this thesis can be found in Appendix 5.1.

2.3 Thermal-FIST

2.3.1 Statistical Hadronization Model

The statistical hadronization model (SHM) describes hadronization using statistical ensembles in dense regions of finite volume, where quarks and gluons interact, forming a QGP state. This QGP state occurs immediately after the initial collision. As the volume of the QGP increases, the temperature decreases. Hadrons are formed from a '*freeze-out*' process in which the QGP state is cooled until thermal and chemical equilibrium is reached locally. This suggests that temperature, T, and the chemical potential, μ, are parameters considered at the equilibrium point or freeze-out. Furthermore, conservation of select quantum numbers (such as baryon number, strangeness, and electric charges) is required to form hadrons[5]. Therefore, in the statistical approach, the dense medium allows all hadrons to be considered in the probability distribution until conservation laws select the appropriate hadrons to be produced from the freeze-out.

2.3.2 Canonical Statistical Model

The canonical statistical model (CSM) treats quantum number conservation laws differently. Within a finite correlation volume (V_c), the violation of baryon number, strangeness, and electric charges (BSQ) is set to zero, ensuring that BSQ is conserved[8]. The correlation volume (V_c) scales with charged multiplicity and is determined by equation 4:

$$V_c = 3\frac{dV}{dy} \approx 7.2\frac{dN_{ch}}{d\eta} \tag{4}$$

where $\frac{dN_{ch}}{d\eta}$ is the charged multiplicity per unit of η and $\frac{dV}{dy}$ is the volume of the QGP state per unit of rapidity. This results in a charged-hadron suppression, or canonical suppression. The charged hadrons are suppressed in the V_c, as additional oppositely charged hadrons have to be produced to keep $BSQ = 0$. BSQ charges being set to zero cause constraints in the formation of multistrange hadrons in different multiplicity classes. In low multiplicity classes, the V_c is consequently small, suppressing multistrange hadrons as they would require additional strange hadrons to conserve strangeness. Furthermore, a small V_c implies that the total number of hadrons formed in the event is reduced once the freeze-out temperatures have been reached. The opposite is true at higher multiplicities, such that a larger V_c and longer time reaching thermal and chemical equilibrium allow more quarks and gluons to interact to form massive hadrons. The increase in V_c also allows a larger space to produce a large number of hadron and charged-hadron combinations, while keeping $BSQ = 0$. Therefore, the canonical suppression factor is greatly reduced.

In pp collisions, at high multiplicities, the CSM model overestimates the strangeness enhancement. To account for the overestimation, the CSM introduces the strangeness saturation factor γ_s[8]. Since the overestimation occurs at higher multiplicities, γ_s increases with increasing multiplicity, such that:

$$\gamma_s^i = 1 - A\exp\left(-\frac{N_{ch}^i}{B}\right) \tag{5}$$

where $A \approx 0.25$ and $B \approx 59$ are parameters experimentally determined. N_{ch}^i is the multiplicity of charged particles in multiplicity class i, determined by the ALICE Collaboration. γ_s can have a maximum strangeness saturation of 1, resulting in no constraints on the production of strange hadrons.

2.3.3 Parameters

Following the ALICE experiment, the chemical potentials for B, S, and Q, are set to zero along with the BSQ charges[8]. The γ_s parameters A and B are set to 0.25 and 59, respectively. γ_s, temperature, and V_c are all set to be dependent on the multiplicity.
The main Thermal-FIST settings that are considered are the Particle ID's, taken from PDG2020[9]. The Particle ID's set whether the particles are stable or set to decay into their constituent decay particles. In accordance with the ALICE experiment, $K^0, \Lambda, \Xi^0, \Xi^-, \Omega^-$ are set to stable. Important to note, the PDG list in Thermal-FIST does not include K^0_S. Instead, K^0 is set to decay into K^0_S with a 50 percent probability. Therefore, when comparing K^0_S and K^0, K^0_S is scaled by 2. The full settings are provided in Appendix 5.2.

3 Method and Results

This section provides the methodology and results for both PYTHIA and Thermal-FIST. The detectors and pseudorapidity ranges for the collider are explained in Section 3.2. The same parameters are used in this thesis. The determination of the multiplicity classes is presented in Section 3.3. Finally, the PYTHIA and Thermal-FIST analysis methodologies and results are explained in Section 3.4. 80 million events were simulated for PYTHIA, while 40 million events were sufficient for Thermal-FIST. The full event generator settings can be found in the Appendix 5.

3.1 Observable(s)

In the Lund string model, Figure 6 shows the different configurations to produce $\Xi - \bar{\Xi}$ pairs using diquark breaks (cases 1 and 2) and junctions (cases 3 and 4). In all cases, strangeness is conserved by placing strange or antistrange quarks in the neighbouring antistrange or strange quarks, respectively.

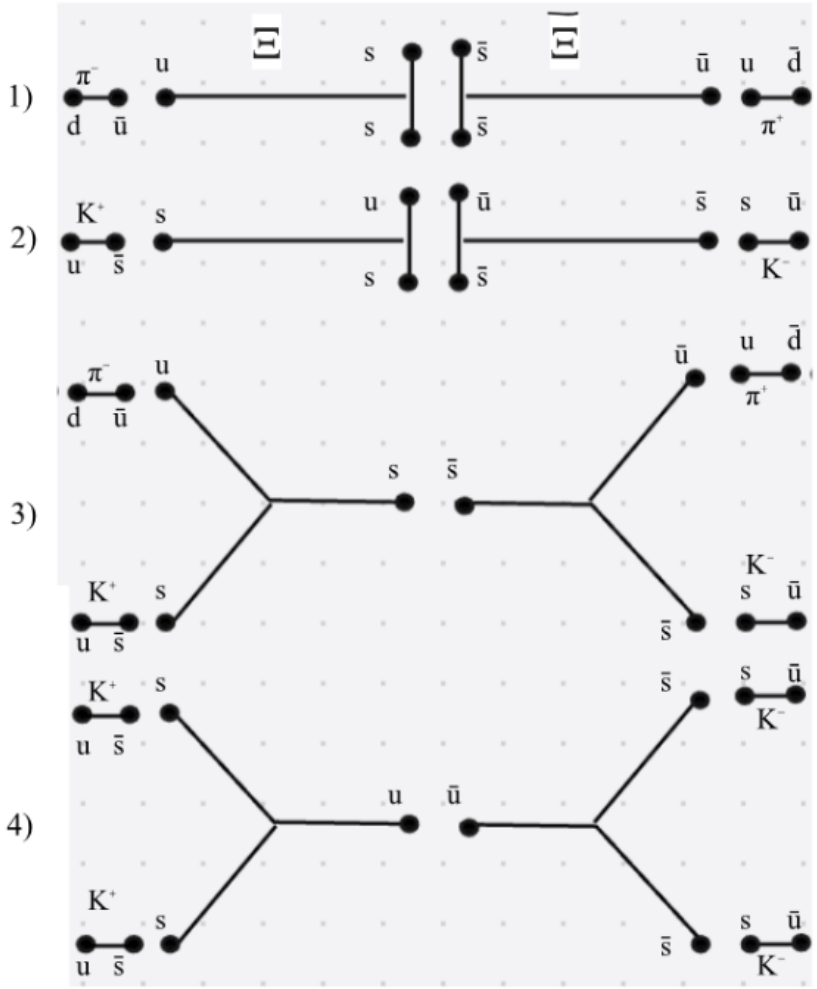

Figure 6: Different configurations of $\Xi - \bar{\Xi}$ and their corresponding kaons.

As seen in Figure 6, three of the possible combinations (cases 2, 3, and 4) require additional kaons produced in association with the $\Xi - \bar{\Xi}$ pair to conserve strangeness.
One may think Ω would have better kaon yields as it has 3 s quarks. However, the production yields decrease with increasing strange quarks in a hadron because of the larger hadron mass and lower probability of strange quark production in the hadronization process for the hadron. Therefore, $\Xi - \bar{\Xi}$ pairs were used as suitable observables for this study.
Since PYTHIA uses the string model and junction dynamics, it requires additional kaons near junction points, leading to rapidity correlations between $\Xi - \bar{\Xi}$ pairs and accompanying mesons. Since Thermal-FIST uses statistical distributions dependent on baryon number and strangeness conservation, $\Xi - \bar{\Xi}$ and their associated kaon productions should yield different results depending on V_c.

3.2 Pseudorapidity, η, and Forward Multiplicity, V_{0M}

A commonly used coordinate in experimental particle physics is the pseudorapidity, η. The pseudorapidity describes the azimuthal angle, θ, of a particle relative to the beam axis in the collider such that:

$$\eta = -\ln\left[\tan\left(\frac{\theta}{2}\right)\right] \tag{6}$$

Figure 7 shows η ranges from $\eta = 0$ to $\eta = \infty$ and $\eta = -\infty$ in relation to the beam axis.

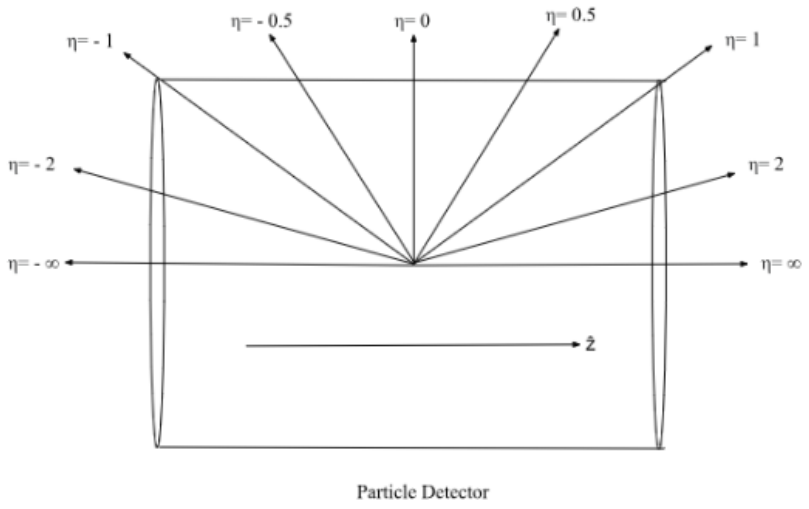

Figure 7: Illustration of the relation between η values with the beam-axis.

The differences in pseudorapidity $\Delta\eta$ between particles are invariant under boosts in the $\hat{z}$-direction (beam axis), making them ideal coordinates in collider experiments. The forward regions in the ALICE experiments[2], backward and forward in the ALICE Coordinate system, correspond to $-3.7 < \eta < -1.7$ and $2.8 < \eta < 5.1$, making angles from $159.28° < \theta < 177.04°$ and $0.687° < \theta < 6.87°$, respectively[1]. These η ranges align with the acceptance of ALICE's two forward ($-3.7 < \eta < -1.7$) and backward ($2.8 < \eta < 5.1$) facing scintillator-based counters called the V_0 detectors (V_{0A} and V_{0C}, respectively) which can then be used to measure the forward multiplicity and determine the event centrality classes. The centrality classes are categorizations of the collision events by the number of charged particles produced in the event.
The forward detectors are scintillator counters where charged hadrons moving through the detectors are recorded. The sum of the charged particles at the V_{0A} and V_{0C} detectors is referred to as V_{0M}, the Forward Multiplicity[10].

3.3 Centrality

The charged-particle multiplicity distribution is used in a forward rapidity region to classify the centralities in a pp collision. The goal is to distinguish events of high activity from low activity. This is done, based on multiplicity, borrowing from "centrality classes" from heavy-ion physics. Although the interpretation in terms of collision geometry is not as straightforward in pp collisions, the terms "multiplicity" and "centrality" classes are used interchangeably. The normalized centrality fraction c for a given event is defined as[11]:

$$c \approx \frac{1}{\sigma_{N_{ch}^{fwd}}} \int_{N_{ch}}^{\infty} \frac{d\sigma}{dN'_{ch,fwd}} dN'_{ch,fwd} \tag{7}$$

where N_{ch}^{fwd} is the number of charged particles in the forward detector acceptance (*forward charged-particle*) for a given event and $\sigma_{N_{ch}^{fwd}}$ is the inelastic cross-section integrated over all possible forward multiplicities (the normalization factor). The cross-section is the probability for a collision to produce a certain number of forward charged-particles. $\frac{1}{\sigma_{N_{ch}^{fwd}}} \frac{d\sigma}{dN'_{ch,fwd}}$ is the probability density as a function of the forward charged-particle multiplicity in the event. The integral computes the cross section for all events with a forward multiplicity greater than or equal to N_{ch}.

The normalized centrality fraction c ranges from 0 (highest multiplicity) to 1 (lowest multiplicity). The events are then grouped into centrality classes based on the percentiles of the total events in the cross-section.
Each event is checked for charged hadrons in the forward detector acceptance, with a transverse momentum greater than 0.1 GeV/c, and then tracked and stored. Following the ALICE experiment, the charged hadrons in each event are stored in the same multiplicity class bins. The probability density of the forward charged-particle multiplicity is shown in Figure 8. The events are plotted as a function of the sum of charged particles detected in the forward detectors. The centrality classes are divided according to the ALICE experiment and can be seen as vertical lines in the plot, with the highest multiplicity class being Class 10.

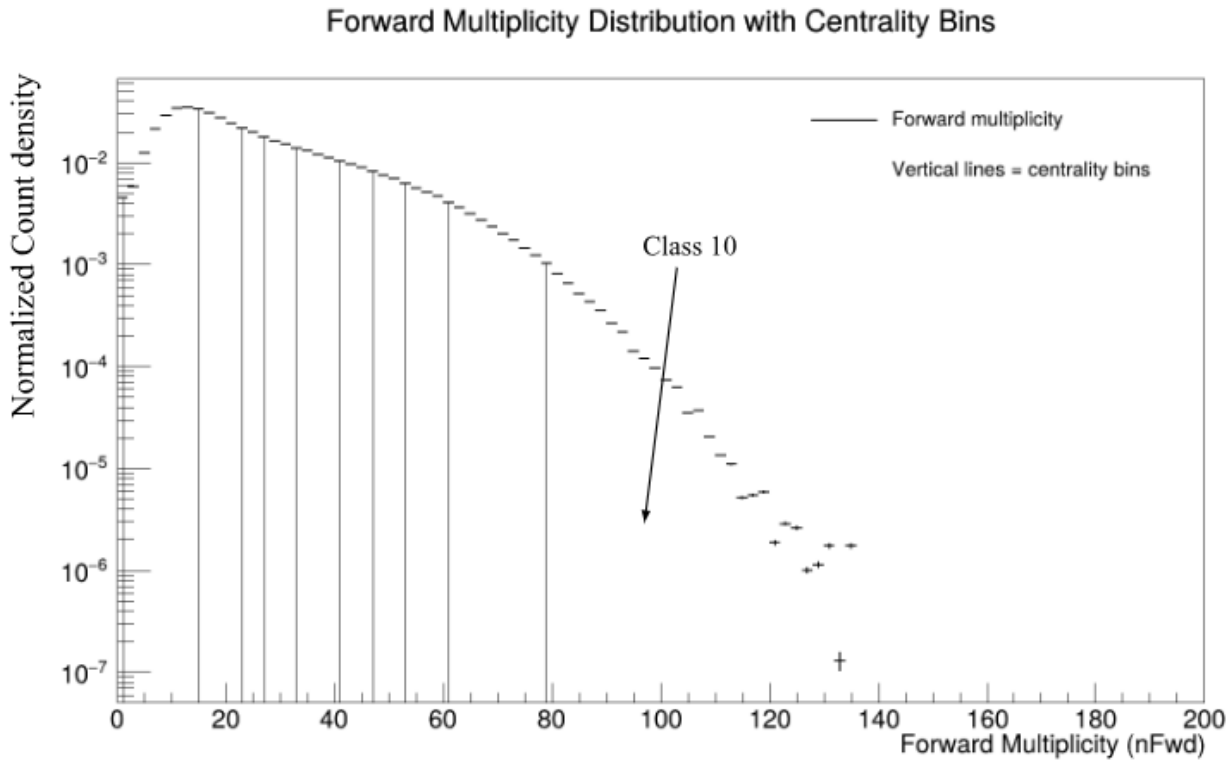

Figure 8: Multiplicity class determination of charged-hadrons in the forward detector acceptance.

3.4 Analysis Methodology and Results

The analysis methodology begins by recreating the strangeness enhancement plot from the ALICE Collaboration, Section 3.4.1. This was done to: (1) validate Monte Carlo settings, (2) validate the centrality calibration, and (3) check whether the parameters used for event generation work as expected. Secondly, in Section 3.4.2, the analysis isolates kaon yields close to $\Xi - \bar{\Xi}$ pairs, normalized to pion yields in the same η range. Finally, in Section 3.4.3, the yields of the respective associated K^+ and K^- of Ξ and $\bar{\Xi}$ baryons are normalized to π^+ and π^-, respectively.
The simulated data from PYTHIA and Thermal-FIST are stored in ROOT files. CERN's ROOT is the standardized software used for high-energy physics (HEP) data analysis[12]. ROOT is used to analyze large datasets from HEP experiments (like ALICE) and Monte Carlo event generators. Hence, ROOT is used throughout the analysis.
The callibration histogram from Section 3.3 is used to compute the centrality percentiles and to define the centrality classes. In accordance with the ALICE experiment[2], the multiplicity

classes are determined by the percentiles of the total event multiplicities, shown in Table 1. The correlation volumes, V_c, were calculated[13] and tabulated according to their respective multiplicity class from lowest to highest in the same table.

Multiplicity class	1	2	3	4	5	6	7	8	9	10
Percentiles	100-68	68-48	48-38	38-28	28-19	19-14	14-9.5	9.5-4.7	4.7-0.95	0.95-0
V_c (fm^3)	18.00	25.20	32.40	45.36	57.60	72.00	99.00	116.64	144.00	187.20

Table 1: Multiplicity class determination according to ALICE Collaboration. Correlation volumes were calculated for convenience.

3.4.1 Strangeness Enhancement: Final-state Hadron to Pion Yield Ratio

This analysis section aims to recreate the strangeness enhancement observed by the ALICE experiment using PYTHIA and Thermal-FIST. The pp collision is set at a center of mass energy of $\sqrt{s} = 7$ TeV. The ALICE Collaboration selected K^0_S, $\Lambda + \bar{\Lambda}$, $\Xi^- + \bar{\Xi}^+$, and Ω^- hadrons normalized to the $\pi^+ + \pi^-$ yield at mid-rapidity $|\eta| < 0.5$ in each multiplicity class. Due to low yields, the strange and multistrange hadrons are scaled as follows: $2K^0_S$, 2Λ, 6Ξ and 16Ω. It is important to recall Section 2.3.3 for Thermal-FIST, K^0 is set to stable, but it is accounted for by halving the scaling factor. This does not affect the final results but simply corrects the missing observable in Thermal-FIST.
The strange and multistrange hadrons are then plotted on a histogram.

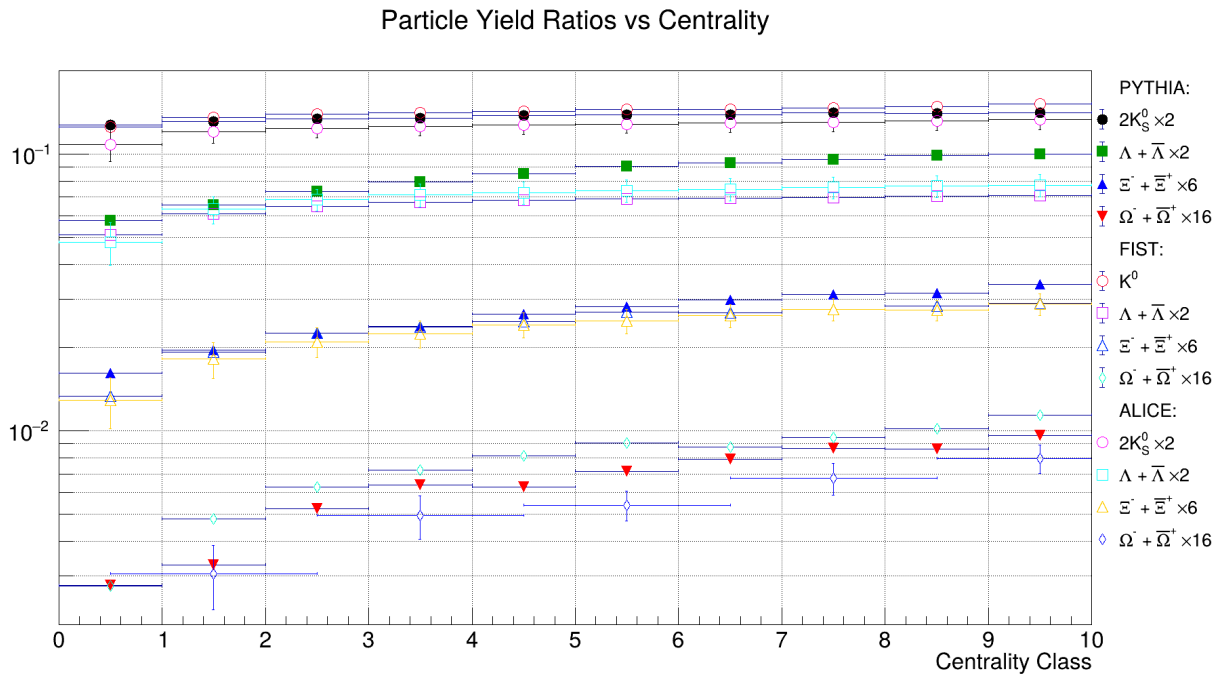

Figure 9: Plot for PYTHIA and Thermal-FIST generated $(K^0_s, \Lambda + \bar{\Lambda}, \Xi^- + \bar{\Xi}^+, \Omega^- + \bar{\Omega}^+)/(\pi^+ + \pi^-)$ yields compared to data from the ALICE experiments, as a function of multiplicity class

Figure 9 shows the selected strange hadron-to-pion yields from the ALICE experiment with simulated data from PYTHIA and Thermal-FIST. The plot has been created as a function of multiplicity class determined in Section 3.3. Both the rope and the statistical hadronization models agree with the experimental data, showing strangeness enhancement at higher multiplicities. Therefore, Figure 9 validates both models, such that they are consistent with the experimental data from the ALICE Collaboration. Thus, the parameters and calibration

method used in this analysis are correct, and further analysis can proceed.
However, PYTHIA slightly overestimates the Λ/π yields, and Thermal-FIST has a higher overestimation of Ω/π yields than PYTHIA at higher multiplicities. For PYTHIA, this might suggest that there are more iterative string breaks in the simulation configuration. The overestimation can be corrected by decreasing the transverse radius of the string, r_0. The parameter r_0, found in Appendix 5.1, sets the string width, typically set at 0.5fm. A smaller r_0 reduces the probability of strings overlapping, leading to fewer and weaker rope formations. In Thermal-FIST, at higher multiplicities, the probability of producing strange hadrons becomes as likely as producing any other hadron (following parameters) as the strangeness saturation factor (γ_s) approaches 1. This may explain the overestimation in Ω/π yields.
The order of the yield ratios reflects the relative production rates of particles with different masses and quark content. It can be seen in Figure 9 that production yields decrease with increasing mass of strange hadrons. For example, the K/π yields are much larger than the Ω/π yields. In PYTHIA, this is because a kaon has one strange quark and a light quark ($K^0_S = s\bar{d}$ or $\bar{s}d$) while the Ω baryon contains three s quarks ($\Omega = sss$). In the simplest case, for a Λ baryon, the probability of one massive s quark *and* one ud diquark tunneling through the potential barrier is given by the strangeness suppression, ρ, and the diquark suppression, ξ, provided in equation (3). The probability of producing a Λ baryon becomes $\rho * \xi$. On the other hand, the probability of producing a Ξ requires a s quark and a su diquark. The probability then becomes $\rho * \xi * \rho$, decreasing the Ξ baryon yield. In Thermal-FIST, the hadron yields are determined by the statistical weight $\exp\left(-m/T\right)$, where m is the mass of the hadron and T is the freeze-out temperature[5]. Therefore, heavier hadrons are canonically suppressed compared to lighter ones. Producing an Ω baryon would require, for example, three kaons to conserve strangeness elsewhere in the V_c, which is statistically unlikely at lower multiplicities. This leads to a hierarchy similar to PYTHIA, whereby $K/\pi > \Lambda/\pi > \Xi/\pi > \Omega/\pi$, but the mechanism is statistically determined in the V_c.

3.4.2 $(K^+ + K^-)/(\pi^+ + \pi^-)$ yields near $\Xi - \bar{\Xi}$ pair

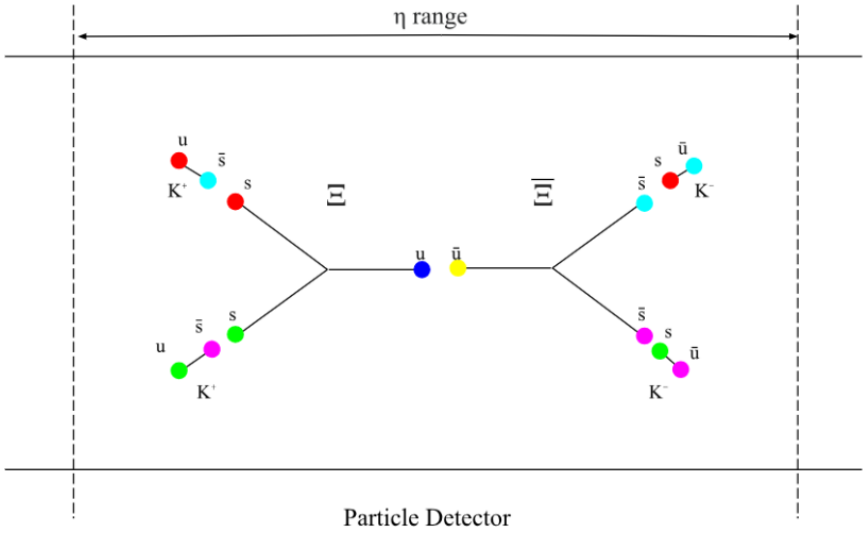

Figure 10: Illustration of obtaining K/π near $\Xi - \bar{\Xi}$ pair.

Only events with $\Xi - \bar{\Xi}$ inclusive pairs in different pseudorapidity ranges are considered. Primarily, the pseudorapidity range is set at $|\eta| < 1$ so that only the specified hadrons within the full detector acceptance at mid-rapidity are accepted. Once the $\Xi - \bar{\Xi}$ inclusive events are

stored, the events are checked again for $K^+ + K^-$ and $\pi^+ + \pi^-$ mesons and stored in a yields file. The file is then used to plot a histogram for the K/π yield as a function of multiplicity class.
Figure 10 shows the analysis methodology for finding kaons and pions in $\Xi - \bar{\Xi}$ inclusive events. This type of analysis requires a large amount of statistics, as finding a $\Xi - \bar{\Xi}$ pair in an event is rare.
In PYTHIA, it can be predicted that, in low multiplicity events, the kaons produced must be related to the production of $\Xi - \bar{\Xi}$ pairs. The production of a massive baryon in a low multiplicity event restricts the possibility of multiple iterative string breaks, like in junction dynamics in Section 2.2.2. Therefore, the $\Xi - \bar{\Xi}$ pair has to be formed via the popcorn model in Section 2.2.1 with a high probability. The $\Xi - \bar{\Xi}$ pair would look like cases (1) and (2) in Figure 6. Case (2), in this situation, would be the only $\Xi - \bar{\Xi}$ combination that requires additional strange mesons to conserve strangeness. In high multiplicity events, where multiple iterative string breaks can occur in the junction legs, the cases (3) and (4) in Figure 6 would be prevalent.
Tracking kaons around $\Xi - \bar{\Xi}$ pairs and normalizing them against pions in the same rapidity range should yield different results between the two models. This is because statistical hadronization requires strangeness to be conserved in the V_c for $B\bar{B}$ pairs. The statistical model would account for the conservation of baryon number and strangeness in the macroscopic system, producing the required hadrons within the η range.

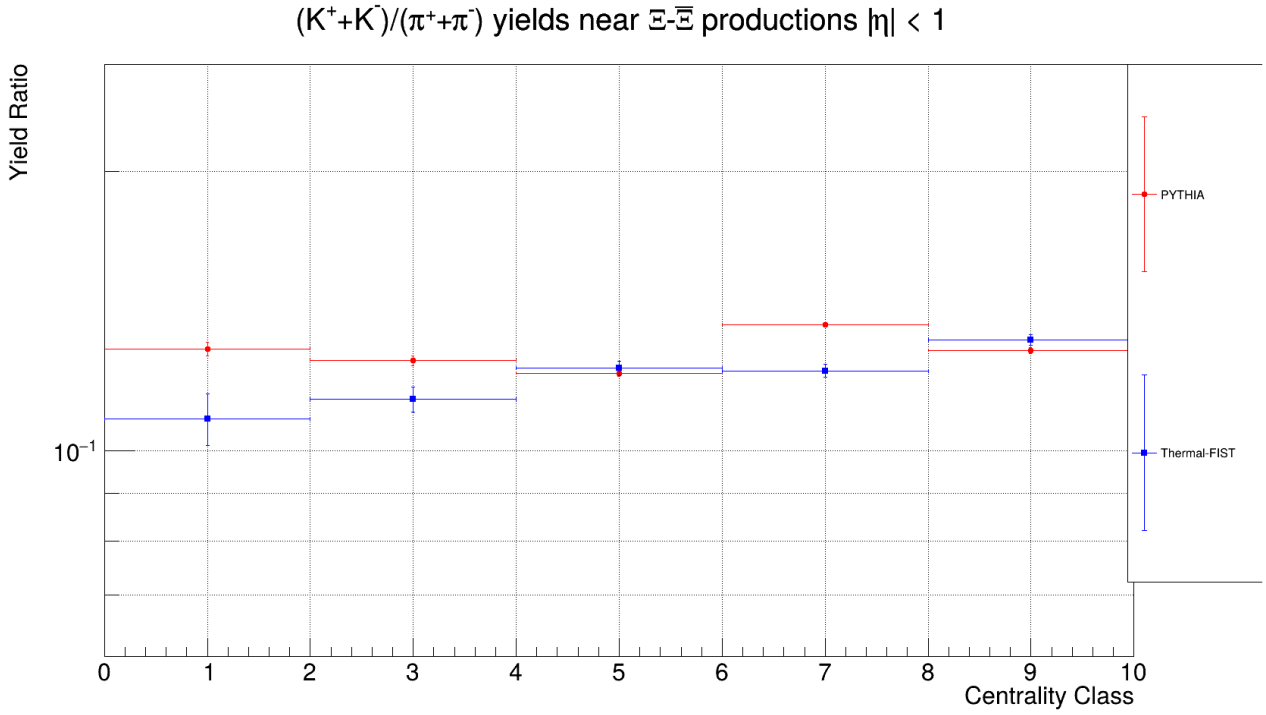

Figure 11: $(K^+ + K^-)/(\pi^+ + \pi^-)$ around $\Xi - \bar{\Xi}$ pair productions at $|\eta| < 1$.

Figure 11 shows the $(K^+ + K^-)/(\pi^+ + \pi^-)$ yields plot around $\Xi - \bar{\Xi}$ pairs as a function of multiplicity class. At first glance, it is clear that the data is insufficient to suggest a strong correlation, even with 80 and 40 million events for PYTHIA and Thermal-FIST, respectively. Hence, the average between two consecutive multiplicity classes was taken to avoid statistical fluctuations in the results. Thermal-FIST shows a slight increase in the K/π yield with increasing multiplicity class. PYTHIA, on the other hand, shows relative flatness across all multiplicity classes, except for the average of the centrality classes 7 and 8, where an increase in K/π yields is observed. This is generally in line with the overall expectation of strangeness

enhancement with increasing multiplicity. However, the final bin seems to decrease again, for which there is no mechanism. Further studies are needed to determine whether this is a physical effect that is observed at higher multiplicities or if the sudden increase in K/π yields may be a statistical fluctuation. This suggests that no strangeness enhancement is observed in the K/π yield across the multiplicity classes.
For PYTHIA, a higher K/π yield is observed at low multiplicities than Thermal-FIST. Since the K/π yields were measured under the condition of $\Xi - \bar{\Xi}$ inclusive events, only 3/4 of the cases in Figure 6 produce the associated kaons to the $\Xi - \bar{\Xi}$ pair. This may suggest that junction-antijunction pairs may also form at low multiplicities. Considering the possibility of diquark breaks and junction-antijunction pairs at low multiplicities would increase the likelihood of kaon production through string breaks. Experimental research of K/π ratios in $\Xi - \bar{\Xi}$ inclusive events at low multiplicities is required to verify whether PYTHIA correctly predicts kaon yields at low multiplicities. On the other hand, at lower multiplicity classes, the strangeness saturation factor, γ_s, is approximately 0.75. In addition to canonical suppression, this maximally suppresses the production of strange hadrons. Furthermore, the probability of having a $\Xi - \bar{\Xi}$ pair in a low-multiplicity event is small, resulting in large error bars at low multiplicities, even with 40 million events. Thermal-FIST follows expectations in $\Xi - \bar{\Xi}$ inclusive events (at $|\eta| < 1$) such that it conserves the strangeness globally. The strangeness enhancement can be explained by the increase in V_c and freeze-out temperatures with increasing multiplicity class, and γ_s approaching unity, explained in Section 2.3.2. The kaons are distributed statistically within the V_c, so they may or may not be close to the Ξ and $\bar{\Xi}$ pairs. Therefore, it does not consider possible combinations of $\Xi - \bar{\Xi}$ pairs that may (cases (2), (3), (4)) or may not (case (1)) require additional kaons in association, as suggested in Section 3.1.

3.4.3 K^+/π^+ and K^-/π^- yield near Ξ and $\bar{\Xi}$, respectively

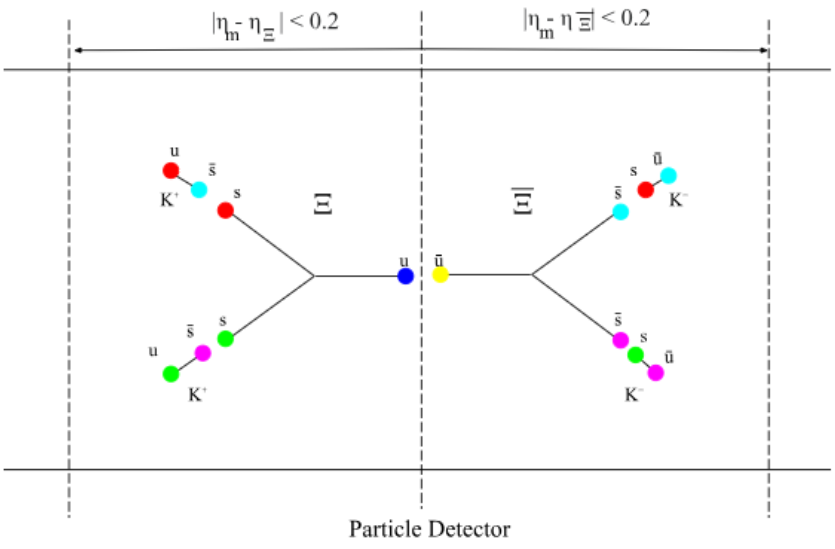

Figure 12: Illustration of obtaining K^+/π^+ near Ξ (left) and K^-/π^- near $\bar{\Xi}$ (right).

Figure 12 extends Section 3.4.2 by illustrating the schematics for obtaining the neighbouring K/π near Ξ and $\bar{\Xi}$, separately. Using the same method as in Section 3.4.2, the events are checked for $\Xi - \bar{\Xi}$ pairs primarily at $|\eta| < 1$ to track hadrons in the full acceptance of the detector in the mid-rapidity range. However, in this section, the aim is to isolate Ξ and $\bar{\Xi}$ and obtain their subsequent neighbouring kaons.

Each event track with a Ξ and a $\bar{\Xi}$ is stored to be further analyzed. The η_{Ξ} and $\eta_{\bar{\Xi}}$ for Ξ and $\bar{\Xi}$ inclusive events are stored accordingly. These event tracks are analyzed once more, whilst ensuring that all hadrons in the event track are within the full detector acceptance rapidity range.

To isolate the baryon and antibaryon, the schematics in Figure 12 is drawn to facilitate the method. The hadrons are situated somewhere in the detector acceptance range. In the case of Ξ, the η_m for the meson is then subtracted from the corresponding η_{Ξ}. If the difference $|\eta_m - \eta_{\Xi}| < 0.2$ (see Figure 7 for reference), then the meson is within $\eta < 0.2$ of the Ξ baryon. This meson can then be recorded and analyzed. Varying this η can now increase or decrease the range of detection for mesons from the Ξ baryon. The same procedure can be applied to the $\bar{\Xi}$ antibaryon.

The selection of the mesons is taken from the illustration for the $\Xi - \bar{\Xi}$ pair combinations in Figure 6. Cases (2) to (4) require additional strange quark/antiquarks to conserve strangeness. The production of multistrange hadrons at the string ends is improbable due to the low probability from the strangeness suppression factor in equation (3). Additionally, the Λ baryon is not considered because the production of another strange baryon neighbouring the rarely occurring $\Xi - \bar{\Xi}$ baryon-antibaryon pair is highly unlikely. Therefore, the hadrons with the highest probability of being produced to conserve strangeness are the K^+ and K^- mesons. The rate of production of K^+ and K^- mesons is then normalized to π^+ and π^- mesons in the same η range. Normalizing kaons to pions of the same charge allows experimental convenience when measuring quark-level probes, such that K^+/π^+ ratios measure $\bar{s}/\bar{d}$ productions and K^-/π^- ratios measure s/d productions. This can then be directly compared to both PYTHIA and Thermal-FIST.

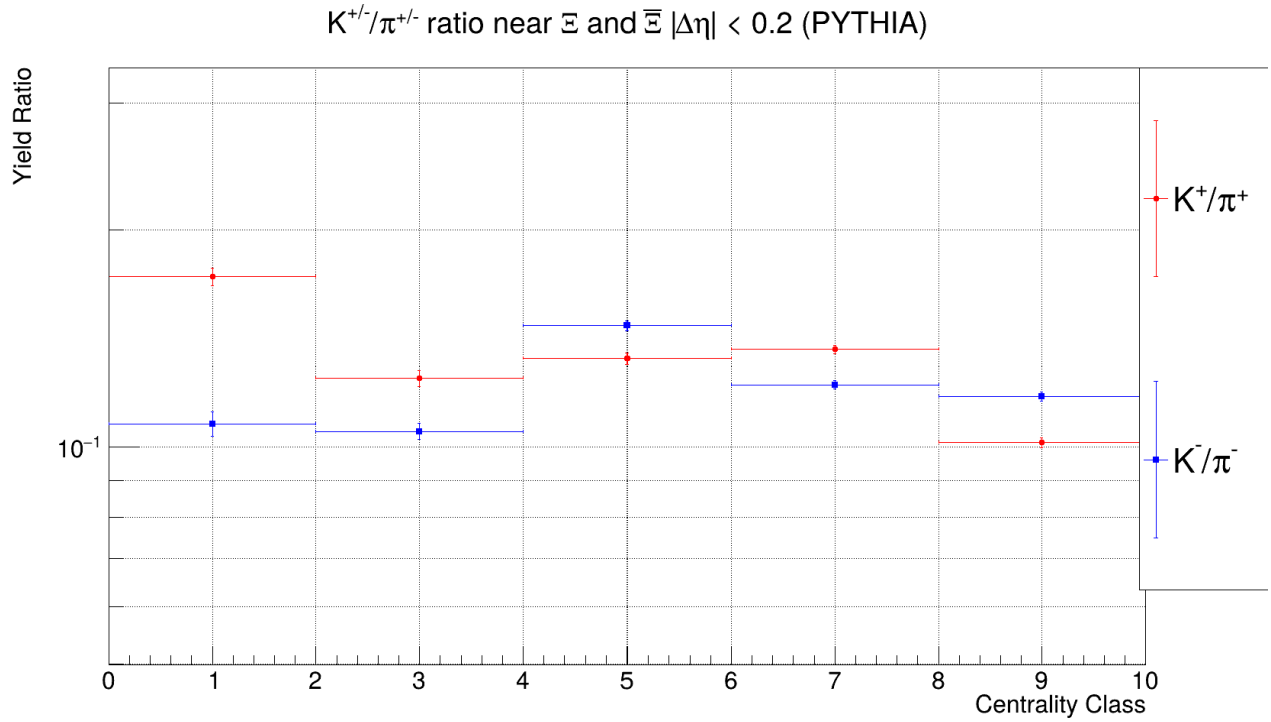

Figure 13: K^+/π^+ and K^-/π^- ratio at $|\Delta\eta| < 0.2$ in PYTHIA.

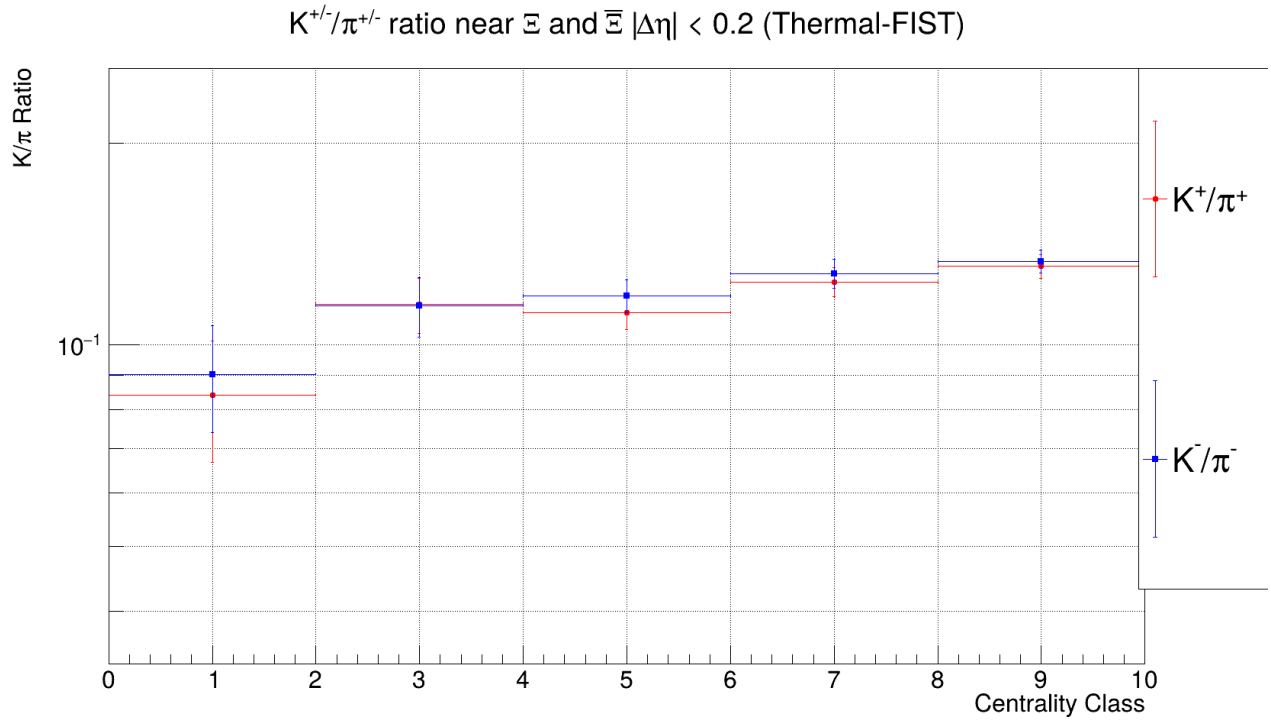

Figure 14: K^+/π^+ and K^-/π^- ratio at $|\Delta\eta| < 0.2$ in Thermal-FIST.

Due to junctions occurring at high multiplicities, referring to Figure 6, K^+ and K^- yields should be equal to each other since a small rapidity range is used $|\eta_m - \eta_\Xi| < 0.2$ and $|\eta_m - \eta_{\bar{\Xi}}| < 0.2$, respectively. However, ϕ and η mesons can also be produced to conserve strangeness. Furthermore, it is expected that a strangeness enhancement would be observed when analyzing the kaon yields against multiplicity in PYTHIA. This is because more rope formations at high multiplicities would increase κ_{eff}, thus increasing the probability of string breaks producing strange hadrons at the outward junction legs.
Similar to Section 3.4.2, Figure 14 shows a low $K^{+/-}/\pi^{+/-}$ yield with large error bars, at low multiplicities. Compared to Figure 11, it can be seen that Thermal-FIST is consistent in showing a small strangeness enhancement with increasing multiplicity class.
On the other hand, in Figure 13 PYTHIA shows larger K^+/π^+ yields than K^-/π^-, significant to the error bars, when averaging between centrality classes 1 and 2, while being relatively flat with increasing multiplicities. This may be because the final-state hadrons at low multiplicities are restricted to conserve charge from the initial state of the pp collision. Hence, when conserving the total charge $Q = +2$ of the two protons in the initial state, one can expect a bias towards positively charged hadrons in the final state to conserve the charge. Furthermore, considering only $\Xi - \bar{\Xi}$ inclusive events creates a further bias towards kaon production to conserve strangeness. Looking at the π productions in case (2) in Figure 6 and considering further associated hadrons at the outward legs using colour confinement and conservation of strangeness and baryon numbers, π^- is associated with K^+ and the opposite for K^-. The charge and strangeness biases can then give a physical interpretation of the effect observed at the low multiplicities. With more data, it may be beneficial to compare with Thermal-FIST whether the same initial-state charge biases are observed at low multiplicities, since there are large error bars at the same centrality classes in Figure 14. Across the higher multiplicities, however, the K^+/π^+ and K^-/π^- yields fluctuate while being relatively flat. A suggestion could be normalizing $K^\pm$ to $(\pi^+ + \pi^-)$. With the inclusion of junction dynamics at higher multiplicities and looking at further associated hadrons from cases (2) to (4) in Figure 6 (producing pions to conserve the baryon number), this modification can increase statistical data and reduce the fluctuations between $K^+/(\pi^+ + \pi^-)$ and $K^-/(\pi^+ + \pi^-)$ yields. This resulted in the following

plots in Figure 15 and 16 for PYTHIA and Thermal-FIST, respectively.

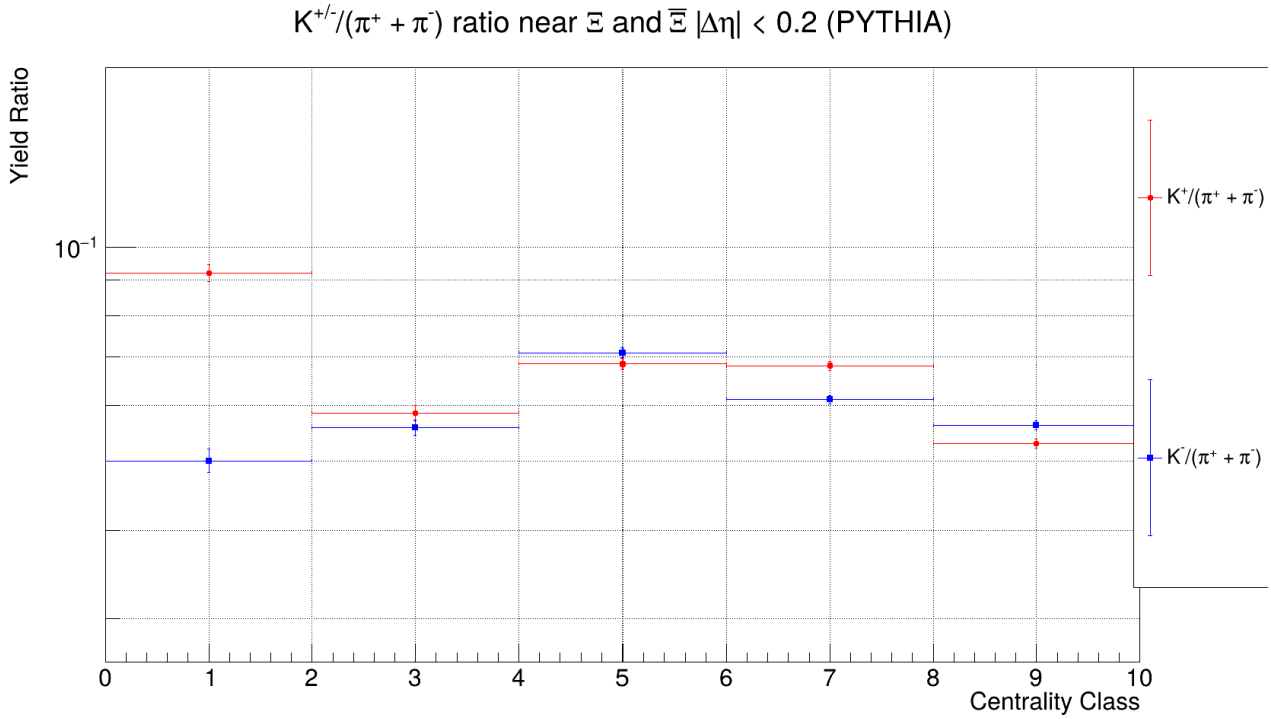

Figure 15: $K^{+/-}/(\pi^+ + \pi^-)$ yield ratio at $|\Delta\eta| < 0.2$ in PYTHIA.

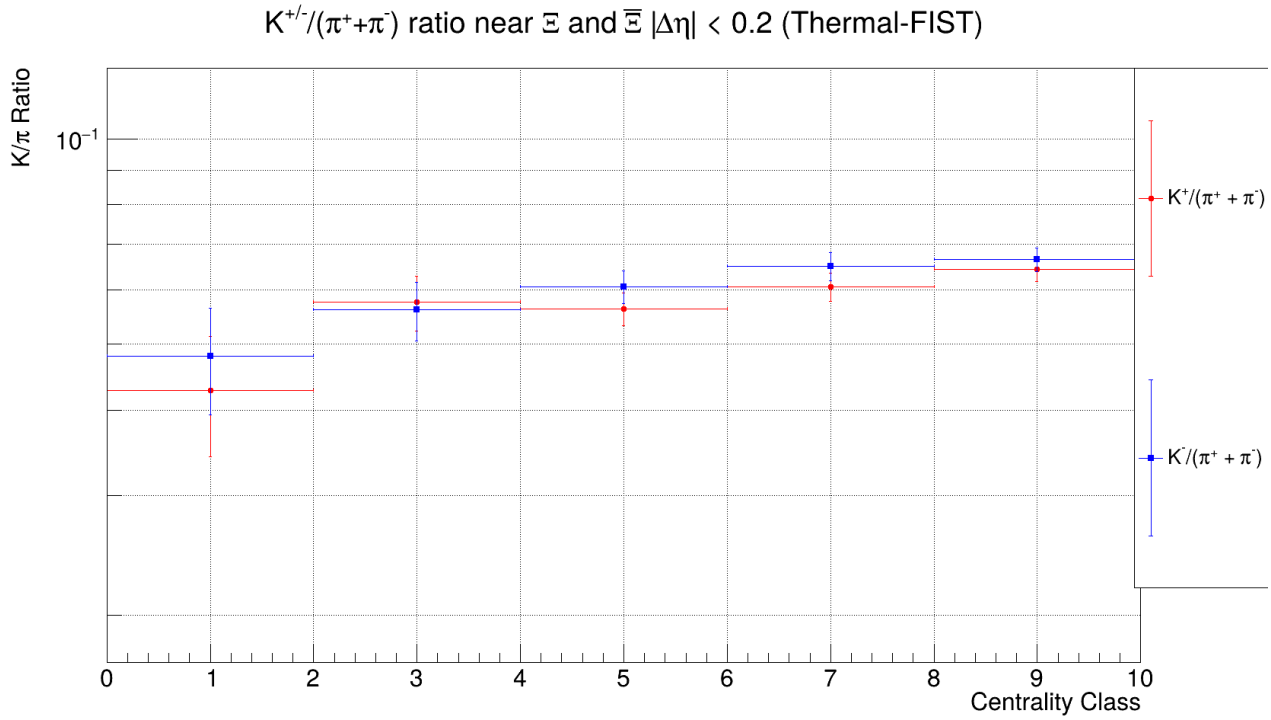

Figure 16: $K^{+/-}/(\pi^+ + \pi^-)$ yield ratio at $|\Delta\eta| < 0.2$ in Thermal-FIST.

Comparing between Figures 13 to 16, it can be seen that the $K^{\pm}$ yields in both PYTHIA and Thermal-FIST are roughly halved when normalizing the $K^{\pm}$ yields to $(\pi^+ + \pi^-)$ at $|\Delta\eta| < 0.2$. In PYTHIA, the lowest multiplicity class in Figure 15 shows similar bias effects for $K^+/(\pi^+ + \pi^-)$ and $K^-/(\pi^+ + \pi^-)$ yields as Figure 13. At higher multiplicities, the $K^+/(\pi^+ + \pi^-)$ and

$K^-/(\pi^+ + \pi^-)$ ratios are relatively equal to each other in their respective centrality class compared to Figure 13. This may suggest the correct diquark breaks and junction dynamics for cases (2), (3), and (4) in Figure 6. The slight fluctuations at higher multiplicities may be the production of other applicable strange mesons associated with the $\Xi - \bar{\Xi}$ pairs, such as ϕ or η mesons. A slight kaon depletion is observed at higher centrality classes (between centrality classes 7-10 in Figure 15), which may suggest a larger number of pions produced from increased string breaks at the outward legs of the junctions. However, the differences in $K^{\pm}/(\pi^+ + \pi^-)$ yields at higher multiplicities are small and may also be the result of statistical fluctuations. Again, further studies are needed to determine whether this is a physical effect that is observed at higher multiplicities. In Figure 16, Thermal-FIST shows increasing $K^+/(\pi^+ + \pi^-)$ and $K^-/(\pi^+ + \pi^-)$ yields with multiplicity. This is due to the strangeness enhancement discussed earlier. Normalizing $K^{\pm}$ to $(\pi^+ + \pi^-)$ roughly halves the production yields since the hadrons are distributed evenly throughout the V_c. Therefore, statistically, it can be seen that $\frac{K^{\pm}}{\pi^{\pm}} \approx \frac{K^{\pm}}{(\pi^+ + \pi^-)/2} = 2\frac{K^{\pm}}{(\pi^+ + \pi^-)}$.

4 Conclusion

This thesis has shown strong agreement between strangeness enhancement, as measured by the ALICE experiment, and the rope and statistical models used by the PYTHIA and Thermal-FIST event generators, respectively. As PYTHIA uses string fragmentation at a microscopic scale to produce $\Xi - \bar{\Xi}$ pairs and their associated mesons and Thermal-FIST uses statistical methods to conserve strangeness within a V_c for $\Xi - \bar{\Xi}$ inclusive events, it was predicted that clear distinctions would be found between the two models. In this paper, it is observed that no significant strangeness enhancement is observed in $K^{\pm}/(\pi^+ + \pi^-)$ yields near Ξ and $\bar{\Xi}$ for both PYTHIA and Thermal-FIST. However, in Figure 15, PYTHIA showed charge and strangeness biases at low multiplicities while a slight kaon depletion at high multiplicities at $|\Delta\eta| < 0.2$. Thermal-FIST, on the other hand, follows the predictions (see Section 3.1) such that it conserves strangeness locally, hence a slight strangeness enhancement is observed with increasing multiplicity in both Figures 11 and 16 as γ_s approaches unity. More research is required to facilitate these claims, using more simulated data and narrower $|\Delta\eta|$ ranges to compare whether Thermal-FIST agrees with the charge bias effects in PYTHIA at low multiplicities. Furthermore, experimental research may help understand the distinctions between the two models at low and high multiplicities.

Further improvements can also be made in the thesis by refining $\Delta\eta$. The orientations of the $\Xi - \bar{\Xi}$ pairs were not considered. Looking at Figure 6, setting the condition that $\eta_{\Xi} < \eta_{\bar{\Xi}}$, the $\Xi - \bar{\Xi}$ pair orientations shown in the figure can be seen. Conversely, $\eta_{\bar{\Xi}} < \eta_{\Xi}$ would have orientations flipped in the opposite direction, such that it would be $\bar{\Xi} - \Xi$ pairs. Then, by isolating Ξ and $\bar{\Xi}$ even further with varying $|\Delta\eta|$, one could find better associated $K^+/(\pi^+ + \pi^-)$ and $K^-/(\pi^+ + \pi^-)$ yields, respectively. This could help to further distinguish the results between PYTHIA and Thermal-FIST.

References

[1] Shreyasi Acharya et al. "Probing Strangeness Hadronization with Event-by-Event Production of Multistrange Hadrons". In: *Phys. Rev. Lett.* 134.2 (2025), p. 022303. DOI: 10.1103/PhysRevLett.134.022303. arXiv: 2405.19890 [nucl-ex]. (accessed: 11.02.2025).

[2] Jaroslav Adam et al. "Enhanced production of multi-strange hadrons in high-multiplicity proton-proton collisions". In: *Nature Phys.* 13 (2017), pp. 535–539. DOI: 10.1038/nphys4111. arXiv: 1606.07424 [nucl-ex]. (accessed: 11.02.2025).

[3] Christian Bierlich. "String Interactions as a Source of Collective Behaviour". In: *Universe* 10.1 (2024), p. 46. DOI: 10.3390/universe10010046. arXiv: 2401.07585 [hep-ph]. (accessed: 10.03.2025).

[4] Christian Bierlich et al. "A comprehensive guide to the physics and usage of PYTHIA 8.3". In: *SciPost Phys. Codebases* (2022), p. 8. DOI: 10.21468/SciPostPhysCodeb.8. URL: https://scipost.org/10.21468/SciPostPhysCodeb.8. (accessed: 10.03.2025).

[5] Volodymyr Vovchenko and Horst Stoecker. "Thermal-FIST: A package for heavy-ion collisions and hadronic equation of state". In: *Comput. Phys. Commun.* 244 (2019), pp. 295–310. DOI: 10.1016/j.cpc.2019.06.024. arXiv: 1901.05249 [nucl-th]. (accessed: 10.03.2025).

[6] Christian Bierlich et al. "Effects of Overlapping Strings in pp Collisions". In: *JHEP* 03 (2015), p. 148. DOI: 10.1007/JHEP03(2015)148. arXiv: 1412.6259 [hep-ph]. (accessed: 10.03.2025).

[7] B Andersson, G Gustafson, and T Sjöstrand. "Baryon Production in Jet Fragmentation and -Decay". In: *Physica Scripta* 32.6 (Dec. 1985), p. 574. DOI: 10.1088/0031-8949/32/6/003. URL: https://dx.doi.org/10.1088/0031-8949/32/6/003. (accessed: 10.03.2025).

[8] Volodymyr Vovchenko, Benjamin Dönigus, and Horst Stoecker. "Canonical statistical model analysis of $p-p$, p-Pb, and Pb-Pb collisions at energies available at the CERN Large Hadron Collider". In: *Phys. Rev. C* 100 (5 Nov. 2019), p. 054906. DOI: 10.1103/PhysRevC.100.054906. URL: https://link.aps.org/doi/10.1103/PhysRevC.100.054906. (accessed: 10.03.2025).

[9] S. Navas et al. "Review of particle physics". In: *Phys. Rev. D* 110.3 (2024), p. 030001. DOI: 10.1103/PhysRevD.110.030001. (accessed: 10.03.2025).

[10] Joyati Mondal et al. "Forward-backward multiplicity and momentum correlations in pp and pPb collisions at the LHC energies". In: *Phys. Rev. D* 107.11 (2023), p. 114016. DOI: 10.1103/PhysRevD.107.114016. arXiv: 2305.07219 [hep-ph]. (accessed: 10.03.2025).

[11] Betty Abelev et al. "Centrality determination of Pb-Pb collisions at $\sqrt{s_{NN}} = 2.76$ TeV with ALICE". In: *Phys. Rev. C* 88.4 (2013), p. 044909. DOI: 10.1103/PhysRevC.88.044909. arXiv: 1301.4361 [nucl-ex]. (accessed: 10.03.2025).

[12] I. Antcheva et al. "ROOT: A C++ framework for petabyte data storage, statistical analysis and visualization". In: *Comput. Phys. Commun.* 182 (2011), pp. 1384–1385. DOI: 10.1016/j.cpc.2011.02.008. (accessed: 10.03.2025).

[13] Volodymyr Vovchenko, Benjamin Dönigus, and Horst Stoecker. "Canonical statistical model analysis of Pb-Pb, and Pb-Pb collisions at energies available at the CERN Large Hadron Collider". In: *Physical Review C* 100.5 (Nov. 2019). ISSN: 2469-9993. DOI: 10.1103/physrevc.100.054906. URL: http://dx.doi.org/10.1103/PhysRevC.100.054906.

5 Appendix

5.1 PYTHIA

The full settings for event generation using PYTHIA8.3 are provided below.

```
! 1) Settings related to the physics processes generated. Here
! a simple pp soft QCD run at 7 TeV.
Beams:idA = 2212        ! first beam p = 2212
Beams:idB = 2212        ! second beam p = 2212
Beams:eCM = 7000.       ! CM energy of collision
SoftQCD:nonDiffractive = on       ! All soft QCD processes are on,

# Set relecant particles to be stable, following the ALICE convention
310:onMode = off
3122:onMode = off
3312:onMode = off
3334:onMode = off
3222:onMode = off
3322:onMode = off
3112:onMode = off

# Parameter of the MPI model to keep total multiplicity reasonable
MultiPartonInteractions:pT0Ref = 2.15

# Parameters related to Junction formation/QCD based CR
BeamRemnants:remnantMode = 1
BeamRemnants:saturation = 5
ColourReconnection:mode = 1
ColourReconnection:allowDoubleJunRem = off
ColourReconnection:m0 = 0.3
ColourReconnection:allowJunctions = on
ColourReconnection:junctionCorrection = 1.2
ColourReconnection:timeDilationMode = 2
ColourReconnection:timeDilationPar = 0.18

# Enable rope hadronization
Ropewalk:RopeHadronization = on

# Also enable string shoving, but don't actually do anything.
# This is just to allow strings to free stream until hadronization
# where the overlaps between strings are calculated.
Ropewalk:doShoving = on
Ropewalk:tInit = 1.5 # Propagation time
Ropewalk:deltat = 0.05
Ropewalk:tShove = 0.1
Ropewalk:gAmplitude = 0. # Set shoving strength to 0 explicitly

# Do the ropes.
Ropewalk:doFlavour = on
```

```
# Parameters of the rope model
Ropewalk:r0 = 0.5 # in units of fm
Ropewalk:m0 = 0.2 # in units of GeV
Ropewalk:beta = 0.1

# Enabling setting of vertex information is necessary
# to calculate string overlaps.
PartonVertex:setVertex = on
PartonVertex:protonRadius = 0.7
PartonVertex:emissionWidth = 0.1


! 2) Settings related to the run
Init:showChangedSettings = on      ! list changed settings
Init:showAllSettings = off         ! list all settings
Init:showChangedParticleData = on  ! list changed particle data
Init:showAllParticleData = off     ! list all particle data
Next:numberCount = 1000            ! print message every n events
Next:numberShowLHA = 1             ! print LHA information n times
Next:numberShowInfo = 1            ! print event information n times
Next:numberShowProcess = 1         ! print process record n times
Next:numberShowEvent = 1           ! print event record n times
Stat:showPartonLevel = on          ! additional statistics on MPI

! 3) Settings related to output.

Main:writeRoot = on            ! Write particle level output to a root file
# Write standard Pythia output to a log file.
Main:outputLog = on             ! Put all printed output to a log file
```

5.2 Thermal-FIST

The full settings for event generation using Thermal-FIST are provided below.

```
constexpr double kVolVsMult = 2.4;
constexpr double kVolOffset = 0.;

const Int_t nMultClasses = 9;
constexpr double kCentClasses[nMultClasses+1] = {0.,    1.,    5.,    10.,   20.,
30.,   40.,   50.,   70.,   100.};
constexpr double kMultCharged[nMultClasses]   = {26.0,  20.0,  16.2,  13.75, 10.0,
8.0,   6.3,   4.5,   2.5};
constexpr double beta_avg[nMultClasses]       = {0.488, 0.44,  0.4,   0.378, 0.325,
0.287, 0.25,  0.20,  0.11};
constexpr double T_kin[nMultClasses]          = {0.163, 0.174, 0.180, 0.181, 0.184,
0.184, 0.183, 0.181, 0.173};
constexpr double n[nMultClasses]              = {1.47,  1.70,  2.01,  2.25,  2.89,
3.48,  4.2,   5.71,  11.6};

constexpr int kNSample = 1;
ThermalModelParameters params;
```

```
\\Chemical potentials are fixed to zero
params.muB = 0.0;
params.muQ = 0.0;
params.muS = 0.0;
params.gammaS = 1.- 0.25 * exp(-kMultCharged[kMultClass] / 59.);
params.gammaq = 1.0;
// Initial temperature value in fits
params.T = 0.176 - 0.0026 * log(kMultCharged[kMultClass]);
// Quantum numbers are zero
params.B = params.Q = params.S = 0;
model->SetParameters(params);
model->SetVolume(kCorrVolume * (kVolVsMult * kMultCharged[kMultClass] + kVolOffset));
model->SetCanonicalVolume(kCorrVolume * (kVolVsMult * kMultCharged[kMultClass]
+ kVolOffset));
model->ConserveBaryonCharge(true);
model->ConserveElectricCharge(true);
model->ConserveStrangeness(true);
// Use quantum statistics
model->SetStatistics(1);
// quantum numbers
model->CalculateQuantumNumbersRange(true);
// resonance width
model->SetUseWidth(ThermalParticle::eBW);
// set chemical potentials
model->FillChemicalPotentials();

// config MC
EventGeneratorConfiguration configMC;
configMC.fModelType = EventGeneratorConfiguration::PointParticle;
configMC.fEnsemble = EventGeneratorConfiguration::CE;
configMC.B = model->Parameters().B;
configMC.Q = model->Parameters().Q;
configMC.S = model->Parameters().S;
configMC.CFOParameters = model->Parameters();

// event generator
CylindricalBlastWaveEventGenerator *generator =
new CylindricalBlastWaveEventGenerator(model->TPS(),configMC);
double betaS = (2. + n[kMultClass]) / 2. * beta_avg[kMultClass];
std::cout << "betaS: " << betaS << std::endl;
generator->SetParameters(T_kin[kMultClass], betaS, kCorrVolume * 0.5, n[kMultClass]);

const Int_t kNumberOfEvents = (kCentClasses[kMultClass+1] -
kCentClasses[kMultClass])*nEventsPerPercent;
    for (int i = 0; i < kNumberOfEvents; ++i){

      nTotalEvents++;
      if (nTotalEvents%1000 == 0) std::cout << "generated " << nTotalEvents <<
      " events..." << std::endl;
```

```
      //      if(i%500)


      auto ev = generator->GetEvent(true);
      SimpleEvent::EventOutputConfig cfg;

      Int_t nAccepted = 0;
      std::vector<SimpleParticle> part = ev.Particles;
      for (auto p : part){ // loop over generated particles

const Int_t absid = TMath::Abs(p.PDGID);
if(absid != 211  && // pi
   absid != 321  && // K
   absid != 310  && // K0s
   absid != 2212 && // p
   absid != 3122 && // lambda
   absid != 3312 && // xi
   absid != 333  && // phi
   absid != 313  && // K*0
   absid != 3334)   // omega
  continue;
```